LA-UR- 10-01358

Approved for public release; distribution is unlimited.

Title:	Application of a four-step HMX kinetic model to an impact-induced friction ignition problem
Author(s):	W. Lee Perry, Jake G. Gunderson, and Peter M. Dickson
Intended for:	14th International Detonation Symposium, April 11-16th 2010, Coeur D' Alene Resort, Idaho

Los Alamos
NATIONAL LABORATORY
EST.1943

Form 836 (7/06)

Application of a Four-Step Kinetic Model to an Impact-Induced Friction Ignition Problem

Background

There has been a long history of interest in the decomposition kinetics of HMX and HMX-based formulations due to the widespread use of this explosive in high performance systems. The kinetics allow us to predict, or attempt to predict, the behavior of the explosive when subjected to thermal hazard scenarios that lead to ignition via impact, spark, friction or external heat. The latter, commonly referred to as 'cook off', has been widely studied and contemporary kinetic and transport models accurately predict time and location of ignition for simple geometries. However, there has been relatively little attention given to the problem of localized ignition that results from the first three ignition sources of impact, spark and friction.

The use of a zero-order single-rate expression describing the exothermic decomposition of explosives dates to the early work of Frank-Kamanetskii in the late 1930s[1,2] and continued through the 60's and 70's. This expression provides very general qualitative insight, but cannot provide accurate spatial or timing details of slow cook off ignition. In the 70s, Catalano, et al., noted that single step kinetics would not accurately predict time to ignition in the one-dimensional time to explosion apparatus (ODTX.)[3] In the early 80s, Tarver and McGuire published their well-known three step kinetic expression that included an endothermic decomposition step.[4] This scheme significantly improved the accuracy of ignition time prediction for the ODTX. However, the Tarver/McGuire model could not produce the internal temperature profiles observed in the small-scale radial experiments[5] nor could it accurately predict the location of ignition. Those factors are suspected to significantly affect the post-ignition behavior and better models were needed. Brill, et al. noted that the enthalpy change due to the beta-delta crystal phase transition was similar to the assumed endothermic decomposition step in the Tarver/McGuire model.[6] Henson, et al., deduced the kinetics and thermodynamics of the phase transition,[7] providing Dickson, et al. with the information necessary to

develop a four-step model that included a two-step nucleation and growth mechanism for the β-δ phase transition.[5] Initially, a irreversible scheme was proposed. That model accurately predicted the spatial and temporal cook off behavior of the small-scale radial experiment under slow heating conditions, but did not accurately capture the endothermic phase transition at a faster heating rate. The current version of the four-step model includes reversibility and accurately describes the small-scale radial experiment over a wide range of heating rates.

While the accuracy of these kinetic schemes has been well tested for cook off, the same cannot be said for the application to much faster hot-spot heating mechanisms. We present here the application of the four step reversible kinetic schemes to an impact-induced friction ignition problem. The results provide insight into the problem of an explosive dropped onto a gritty surface. This ignition mechanism has been implicated in several accidents and continues to be a concern. In this work, we observed the impact of PBX 9501, with grit embedded in its surface, through transparent anvils with an infrared camera to observe the temperature field at the ignition point. Dynamic load data were also acquired such that we could compute the heat applied to the explosive due to friction. This process was modeled using a high- fidelity heat and mass transport code, which employed the reversible four step kinetic scheme. A good model-experiment correlation helps to validate the four-step model in a new spatial and temporal regime.

Development of the Kinetic Scheme and Validation for Slow Cookoff

The simplest kinetic expression is the zero- order single step Arrhenius expression and the heat generated is the product of that rate and the reaction enthalpy. This expression has been used in conjunction with the heat equation since the early days of thermal explosion research. The use of this expression provided the foundations of our understanding of critical ignition conditions, best exemplified by the theories of Frank-Kamenetskii and Seminov. [1,2]

However, Catalanon's observation that the zero-order single step expression failed to accurately predict the time to explosion the ODTX experiment led Tarver and

McGuire to develop the three-step expression. They developed their model based on the knowledge of the proposed chemical reaction steps that occur during the explosion process and suggested that three rate-limiting steps controlled the overall process. Their model was therefore a 3-step Arrhenius scheme to describe the slow thermal decomposition of HMX, which has been very successful in predicting time-to-explosion for HMX-based explosives over a wide range of heating rates. The scheme involves the following reactions, in which the composition of the fragments and intermediate products is unspecified, and although the framework was based on likely chemical steps, it is basically a multi-parameter curve fit to the ODTX experiments.

1. HMX $\rightarrow$ *fragments*

   (1st order endothermic)

2. *fragments* $\rightarrow$ *intermediate gases*

   (1st order exothermic)

3. *intermediate gases* $\rightarrow$ final products

   (2nd order exothermic)

Despite the success of this scheme in predicting time to explosion, it failed to accurately predict the internal temperature behavior of the Los Alamos Small-Scale Radial cook off test (SSR), which provided time-resolved internal temperature profiles.[5] This was significant, as ignition location within the charge and the temperature distribution prior to ignition are factors recognized to strongly influence reaction violence.

In order to address this problem, we made some modifications to the scheme and adjusted the thermal properties of PBX 9501 slightly as required to model the experimental data. The model was developed using a 1-D / 2-D axi-symmetric / 3-D spherically symmetric, explicit finite difference code, 2nd order accurate in space and

time. It was also tested using implicit Abaqus and Mathematica codes. We tested these model results against the ...

Brill et al.[6] made kinetic measurements of the HMX β to δ phase transition, and showed that the kinetic parameters were similar to those attributed to the decomposition kinetics. Recent work[7] has shown that the first endothermic step in the McGuire-Tarver model, which was introduced to give the correct induction time behaviour, does broadly represent the β to δ phase transition in HMX. This endotherm causes the dip in the temperature record at around 170 °C, but it is not well represented by first order Arrhenius kinetics. We use a combination of first order and bimolecular forms of the thermodynamic formulation of conventional transition state theory (TST) kinetics to represent the nucleation and growth process of the transition, with an overall transition energy very similar to that used in the previous model. Immediately after the sharp phase transition, comparison with heat-transfer code predictions indicates that a slow endothermic process occurs. A first order Arrhenius step was used to model this. Lastly, a bimolecular exothermic reaction leads to thermal runaway.

1. HMX (β) → HMX (δ)

   (first order endothermic)

2. HMX (β) + HMX (δ) → HMX (δ)

   (bimolecular endothermic)

3. HMX (δ) → *products*

   (1st order endothermic)

4. HMX (δ) + *products* → *products*

   (bimolecular exothermic)

Irreversible phase change version

In the first version of this model,[5] an irreversible description of the phase change was used. The associated rate equations, described in terms of mass fractions, are,

$$\Re_1 = M_a \frac{kT}{h} \exp\left\{\frac{T\Delta S_1 - E_1 - P\Delta V}{RT}\right\} \qquad \text{(phase change nucleation)},$$

$$\Re_2 = M_a M_b \frac{kT}{h} \exp\left\{\frac{T\Delta S_2 - E_2 - P\Delta V}{RT}\right\} \qquad \text{(phase change growth)},$$

$$\Re_3 = M_b Z_3 \exp\left\{\frac{-E_3}{RT}\right\} \qquad \text{(1st order endothermic step)},$$

$$\Re_4 = M_b M_c Z_4 \exp\left\{\frac{-E_4}{RT}\right\} \qquad \text{(bimolecular exothermic step)}. \qquad (1\text{-}4)$$

M_a, M_b and M_c represent the mass fractions of β HMX, δ HMX and products respectively. ΔS, E and ΔV are expressed per mole, and R is the molar gas constant (8.31 J mol^{-1} K^{-1}). The $P\Delta V$ term turns out to be small compared to the other terms in the numerator of the exponential, and in practice may be ignored.

These equations combine to form a coupled set of differential equations describing the rate of change of the mass fractions of each species as follows:-

$$\frac{\mathrm{d}\, M_a}{\mathrm{d}\, t} = -\Re_1 - \Re_2$$

$$\frac{\mathrm{d}\, M_b}{\mathrm{d}\, t} = \Re_1 + \Re_2 - \Re_3 - \Re_4$$

$$\frac{\mathrm{d}\, M_c}{\mathrm{d}\, t} = \Re_3 + \Re_4 \qquad (5\text{-}7)$$

The parameters used in this version were fitted primarily to the early SSR shots (PBX 9501 cylinders, L = 2 in., Ø = 1 in., unsealed, time to phase change ~ 6 ks) are shown in table 1. Note that the kinetic parameters published in the APS proceedings were per kg.

$\Re$ #	Z	ΔS (J mol^{-1} K^{-1})	E (J mol^{-1})	ΔV (m^3 mol^{-1})	ΔH (kJ kg^{-1})
1		136	2.05×10^5	1.40×10^{-5}	– 25
2		630	4.13×10^5	3.61×10^{-6}	– 25
3	3.16×10^{16}		2.00×10^5		– 120
4	8.0×10^{15}		1.74×10^5		3200

Table 1. Kinetic parameters (irrreversible scheme).

Note that the 3rd and 4th reactions are apparently doing the same chemistry (HMX (δ) $\rightarrow$ *products*), and yet have different heats of reaction. This is chemically unrealistic.

We used a linear fit for estimated thermal conductivities and specific heat capacities for HMX β, HMX δ and products as a function of temperature, and compute the thermal conductivity and specific heat capacity of the mixture as a mass-fraction-weighted linear combination:–

$$k_i = a_{ki} + b_{ki}T, \qquad k_{mixture} = \Sigma m_i k_i, \qquad 8$$

$$c_i = a_{ci} + b_{ci}T, \qquad c_{mixture} = \Sigma c_i k_i, \qquad 9$$

where T is the absolute temperature. Table 2 shows the values for the thermal parameters. The high value for the conductivity of the products reflects both conduction and permeation of hot gas, both of which are probably occurring.

i	a_k (J m^{-1}K^{-1}s^{-1})	b_k (J m^{-1}K^{-2}s^{-1})	a_c (J kg^{-1}K^{-1})	b_c (J kg^{-1}K^{-2})
1	1.42	-2.08×10^{-3}	236	2.7
2	0.53	-5.40×10^{-4}	236	2.7
3	2.0	0.0	222	2.45

Table 2. (Thermal parameters irreversible scheme).

Figure 1 shows the comparison of the model with the centre thermocouple record for a representative SSR shot where we used a heating rate of xxx. Note in particular that the fit through the phase change is reasonable. The onset, duration and depth of the endotherm are all captured quite well. However, subsequent shots heated at a faster rate through the phase change produced a rather poorer match. Figure 2 shows the model comparison with shot where the heating rate was xxx.

Reversible phase change version

Further data from SSR experiments with faster ramps, and data acquired using laser second harmonic generation and Raman spectroscopy to probe the phase change in both PBX 9501 and HMX[8] indicated that a reversible description of the nucleation and growth model is required to reproduce observed behaviour. As a result, the first two steps were modified thus:-

$$\Re_1 = M_a \frac{kT}{h}\exp\left\{\frac{T\Delta S_{1f} - E_{1f} - P\Delta V}{RT}\right\} - M_b \frac{kT}{h}\exp\left\{\frac{T\Delta S_{1r} - E_{1r} - P\Delta V}{RT}\right\},$$

$$\Re_2 = M_a M_b \frac{kT}{h}\left(\exp\left\{\frac{T\Delta S_{2f} - E_{2f} - P\Delta V}{RT}\right\} - \exp\left\{\frac{T\Delta S_{2r} - E_{2r} - P\Delta V}{RT}\right\}\right),$$

$$\Re_3 = M_b Z_3 \exp\left\{\frac{-E_3}{RT}\right\},$$

$$\Re_4 = M_b M_c Z_4 \exp\left\{\frac{-E_4}{RT}\right\}. \qquad (10\text{-}13)$$

The associated parameters, shown in table xx, were optimized by comparison with the phase change experiments and the later SSR experiments using a linear, and faster temperature ramp (~ 2ks to phase change).

$\Re$#	Z	ΔS_f (J mol^{-1} K^{-1})	E_f (J mol^{-1})	ΔV (m^3 mol^{-1})	ΔH (kJ kg^{-1})	ΔS_r (J mol^{-1} K^{-1})	E_r (J mol^{-1})
1		123.0	2.040×10^5	4.73×10^{-5}	- 25	89.0	1.890×10^5
2		-40.37	1.015×10^5	1.22×10^{-5}	- 25	-75.2	8.650×10^4
3	3.16×10^{16}		2.000×10^5		- 120		
4	8.00×10^{15}		1.731×10^5		3200		

This scheme reproduces the faster phase changes much better. Figure 3 shows the comparison with an experiment that used a ramp rate of xxx. However, it does less well on the slower shots; figure 4 shows the comparison with a shot that used a ramp rate of xxx.

The sensitivity of these models to various parameters has been explored. The ignition point is particularly sensitive to the activation energy, and, to a lesser extent, the exothermicity of the final step. It should be noted that there are generally a number of ways to achieve a fit to any given data set in the ignition region. The phase change is more constrained, and there is clearly either an oversimplification in the reversible model, or other changes are happening that alter the kinetics. It has been proposed that the presence of the plasticizer modifies the

phase change kinetics. Evidence for this has been found in comparing the response of PBX 9501 and HMX crystals with and without plasticizer. During slow heating, the plasticizer may be driven off, leading the PBX 9501 to behave more like pure HMX. With these caveats in mind, we conclude the reversible four-step scheme provides a true chemistry based model that successfully describes slow cook off over a range of heating times. We now review our efforts towards validating this model for the fast, localized hot-spot heating problem of impact-induced friction with grit present.

The Impact-induced Friction Experiment

An instrumented vertical-drop impact machine having transparent anvils provided the platform for these experiments, and more detail can be found in another publication.[9] Figure 5 shows a schematic of the rail cart and anvil assembly at impact where the infrared camera views one side of the sample. A photodiode detected ignition and was used as a fiducial. The moving anvil was a calibrated load cell such that circumferentially mounted strain gauges provided axial loading during an impact event. The 2.44 kg rail cart was dropped from 1.6 m such that the nominal impact velocity was 5 m/s and the nominal impact energy was 30.5 J. Optical detectors measured the impact velocity.

The samples were 6.35 mm dia. x 2.5 mm cylinders of PBX 9501. Three 400 micron diameter spherical silica grit particles were embedded in the surface of the sample facing the camera. The sliding velocity of the grit under impact depended on the initial position, which was 1.7 mm from the center of the sample.

A Santa Barbara Focal Plane SBF119 infrared camera (InSb) was used to view the temperature field just prior to ignition. The camera provided the infrared images in the 3.5 - 5.0 μm band. The maximum framing rate (1 kHz) for this camera did not provide sufficient temporal resolution of an impact event (1 ms), so the camera was operated in a single-frame acquisition mode. The spatial resolution was 74 μm per pixel. We sought to acquire images coincident with a specific load value

correlated with ignition, and a Tektronix DPO oscilloscope acquired the strain gauge signal and triggered the camera at a voltage corresponding to the load at ignition.

The camera IR flux was calibrated against a black body source and the emissivity of the silica particles was measured for temperature measurement. The friction coefficient between the silica grit and the sapphire surface was also measured. The friction coefficient was determined to be 0.107.

Results For Impact-Friction Experiments

The four-step reversible kinetic scheme was successful for slow cook off ignition problems; our goal here was to test the efficacy of the model to the much faster ignition problem of impact-induced friction. Figure 6 shows a typical load curve during impact, along with the photodiode signal where ignition occurred at t=0. Note the change in slope of the load curve at ignition as the reaction product gases apply pressure to the anvils. Figure 7 shows an IR image of the grit particle and the surrounding region just prior to ignition at 512 microseconds. This image represents a typical temperature measurement where the IR flux was converted to temperature. The temperature at the time this image was acquired was estimated to be 987 K. Twelve shots were done, and the average time to ignition for all shots (12) was 461 microseconds with a standard deviation of 31.4 microseconds.

Modeling Approach and Results

The general theoretical framework encompassed heat transport, the reversible four step reaction kinetics and heat generation, and heat generated by friction (work). A 2 dimensional numerical model was constructed using the COMSOL Multiphysics modeling package. COMSOL is a modular package, and we employed the heat transport model and the mass transport module. The mass transport module was used to track species consumption as dictated by the kinetic expression. Our approach did not consider the movement of species, and the diffusion coefficient was set to zero. Figure 8 shows the rendering of the system where, at the rearward corner of the grit-substrate interface, a 5 micron air gap was introduced in to represent the smallest dimension occupied by the explosive based on the HMX fine

particle size found in PBX 9501. The contact area between the grit and sapphire was calculated to be 8.4 x 10^{-9} m^2 using Hertzian contact stress analysis.[10] At this interface between the substrate and grit, a heat flux discontinuity boundary condition was imposed using an exponential curve fit of the average work rate. The rate of work done at the grit-substrate interface was the prime driver for the system, and we provide the details of how dynamic load data were reduced to provide this information. In addition to dynamic load, work rate was found from the initial sample dimensions and initial grit location. The impact-induced deformation of the sample caused radial motion of the grit from its original position R_g to a coordinate r, such that there was mechanical work action at the grit-substrate interface. The time-accumulated work done by friction at the grit-lower anvil interface was

$$W = \mu \int_0^t F_N v_g dt \quad , \tag{14}$$

where μ is the friction coefficient, F_N is the normal force applied to the grit, and v_g is the grit velocity. The rate of work done was

$$\dot{W} = \mu F_N v_g \quad . \tag{15}$$

Conservation of volume allowed us to find the evolution of normal stress (σ) during impact, which allowed us to compute F_N and v_g. The transform requires the height of the sample during impact $h(t)$:

$$h(t) = h_0 - \int_{t_0}^{t} \left(v_z(\tau) - v_0\right) d\tau \quad , \tag{16}$$

where h_0 was the initial thickness of the sample and

$$v_z(t) = v_{z0} - \frac{1}{m} \int_{t_0}^{t} F(\tau) d\tau \quad . \tag{17}$$

The radius of the sample evolved as

$$r(t) = r_0\sqrt{\frac{h_0}{h(t)}}, \qquad 18$$

where r_0 was the initial radius of interest (either sample radius R_s or grit location R_g). The grit velocity was

$$v_g = \frac{dr}{dt} = r_0\frac{\sqrt{h_0}}{2h(t)^{3/2}}v_z(t). \qquad 19$$

The normal load on the grit was estimated from the ratio of the axially projected surface area of the grit particle to the sample surface area. This was not a constant value and changed as the sample deformed under impact. The stress was

$$\sigma(t) = \frac{F(t)h(t)}{\pi R_s^2 h_0}, \qquad 20$$

and the normal force on the grit was

$$F_N = F(t)\frac{h(t)}{h_0}\left(\frac{R_g'}{R_s}\right)^2. \qquad 21$$

So that the interfacial work rate was

$$\dot{W} = \mu F(t)\frac{R_g^3}{R_s^2\sqrt{h(t)h_0}}v_z(t). \qquad 22$$

Note the sensitivity of the work rate to the initial grit position. Figure 9 shows the grit velocity for each value of grit normal force corresponding to a measured impact load. Since the velocity was nearly constant through the impact process, we used a uniform tangential thermal velocity field of 1.65 m/s in the sapphire region to emulate the effect of the moving grit. Finally, Figure 10 shows a continuous model of work rate increase during the impact process according to equation 22. To develop this model, a general load curve was computed from the average of the load curves from all experiments. The velocity field (grit velocity) and the work rate were the

essential reduced observations that provided the primary thermal inputs for the simulation.

Model Results

Figure 11 shows a colored contour map at the time of ignition at three different zoom levels.[9] In these images, the grit moved towards the left. Frame a) shows the global model temperature surface map that includes the explosive, the silica grit particle and the sapphire substrate. Frame b) shows a magnification of the grit-sapphire interface. Frame c) highlights the ignition location. The model suggests that residual heat generated by the sliding grit is transported into the trailing explosive and causes ignition. The model also shows that the bead is undisturbed several microns from the heat source (grit-substrate interface.) The model's predicted thermal penetration is consistent with the Fourier number:

$$\tau = \alpha t / D^2 \qquad 23$$

This dimensionless ratio is a product of analytical theory and provides a characteristic relationship time (t) and a characteristic thermal penetration depth (D) for a system having a given thermal diffusivity (α) and the implication here is that the grit size was not important.

Figure 12 shows the predicted temperature-time behavior at the ignition location. The model ignition time was 526 microseconds, which was within 2 σ of the observed average ignition time. The overall reasonable temporal and temperature agreement gives us good confidence in the overall picture provided by the model.

Finally, Figure 13 shows the value of the model heat source term at the ignition location. While the plot shows the endothermic phase transition, the temperature trajectory of the ignition location shown in Figure 12 increases monotonically. This contrasts the results of previous cook off models and may result from the very small length and time scales investigated here.

Conclusions

We have observed impact-induced friction ignition of PBX 9501 with grit embedded between the explosive and the lower anvil surface. Observation was done using an infrared camera looking through the sapphire bottom anvil. Time to ignition and temperature-time behavior were recorded. The time to ignition was approximately 500 microseconds and the temperature was approximately 1000 K.

The four step reversible kinetic scheme was previously validated for slow cook off scenarios. Our intention was to test the validity for significantly faster hot-spot processes, such as the impact-induced grit friction process studied here. We found the model predicted the ignition time within experimental error.

There are caveats to consider when evaluating the agreement. The primary input to the model was friction work over an area computed by a stress analysis. The work rate itself, and the relative velocity of the grit and substrate both have a strong dependence on the initial position of the grit. Any errors in the analysis or the initial grit position would affect the model results. At this time, we do not know the sensitivity to these issues. However, the good agreement does suggest the four step kinetic scheme may have universal applicability for HMX systems.

References

[1] D.A. Frank-Kamenetskii, *Diffusion and Heat Transfer in Chemical Kinetics*, Plenum Press (New York, 1969).
[2] D.A. Frank-Kamenetskii, Zh. Fiz. Khim., 13 (1939) 738.
[3] E. Catalano, R. McGuire, E. Lee, E. Wrenn, D. Ornellas and J. Walton, "The thermal decomposition and reaction of confined explosives," Sixth Symposium (International) on Detonation, White Oak, MD (1976) p214.
[4] McGuire, R.R. & Tarver, C.M., "Chemical decomposition models for the thermal explosion of confined HMX, TATB, RDX, and TNT explosives," Seventh International Symposium on Detonation, Annapolis, MD (1981) p. 56.
[5] P.M. Dickson, B.W Asay, B.F. Henson, C.S. Fugard, J. Wong, "Measurements of phase change and thermal decomposition kinetics during cookoff of PBX 9501," AIP Conference Proceedings, 505 (2000) p.837.

[6] T.B Brill, and R.J. Karpowicz, J. Phys. Chem. 86, (1982) 4260.
[7] B.F. Henson, B.W Asay, R.K. Sander, S.F. Son, J.M. Robinson, and P.M. Dickson, Phys. Rev. Lett. 82 (1999) 1213.
[8] Smilowitz, L.M., Henson, B.F., Asay, B.W, Dickson, P.M., "The beta-delta phase transition in the energetic nitramine octahydro-1,3,5,7-tetranitro-1,3,5,7-tetrazocine", Journal of Chemical Physics, 620(2) (2002) 1069.
[9] Perry, W.L., Gundersion, J.A., Balkey, M.M., and Dickson, P.M. "Impact-induced friction ignition of an explosive: Infrared Observations and Modeling" Submitted to Journal of Applied Physics (2010).
[10] Timonshenko, S.P., and Goodier, J.N., *Theory of Elasticity*, 3rd ed. (McGraw Hill, 1970).

Figure 1

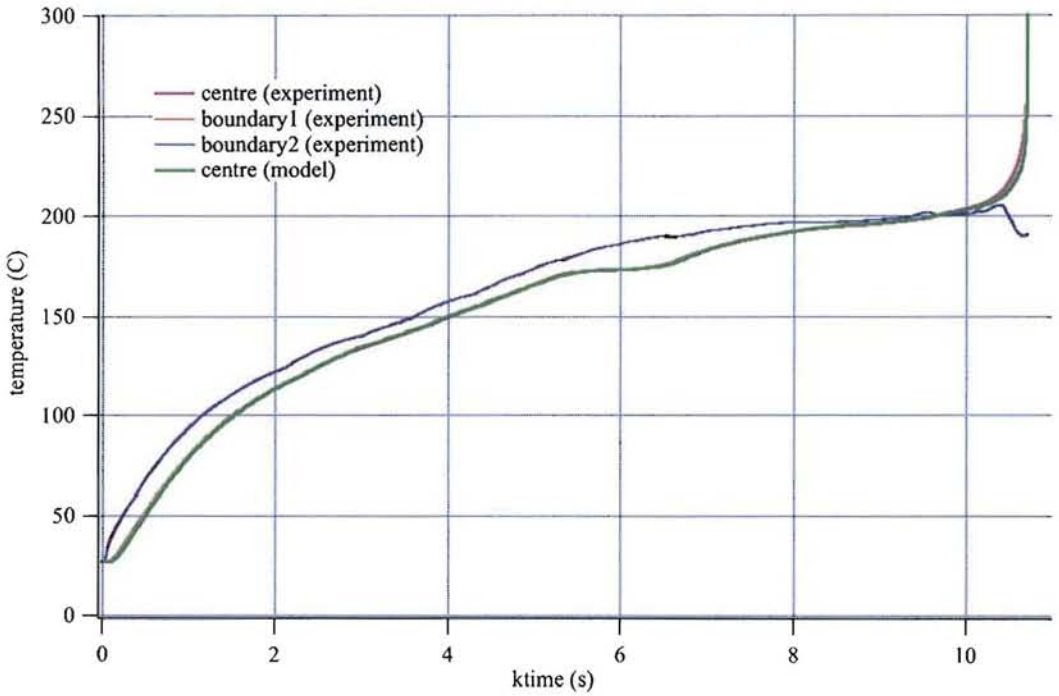
centre (experiment)
boundary1 (experiment)
boundary2 (experiment)
centre (model)
temperature (C)
ktime (s)
300
250
200
150
100
50
0
0
2
4
6
8
10

Figure 2

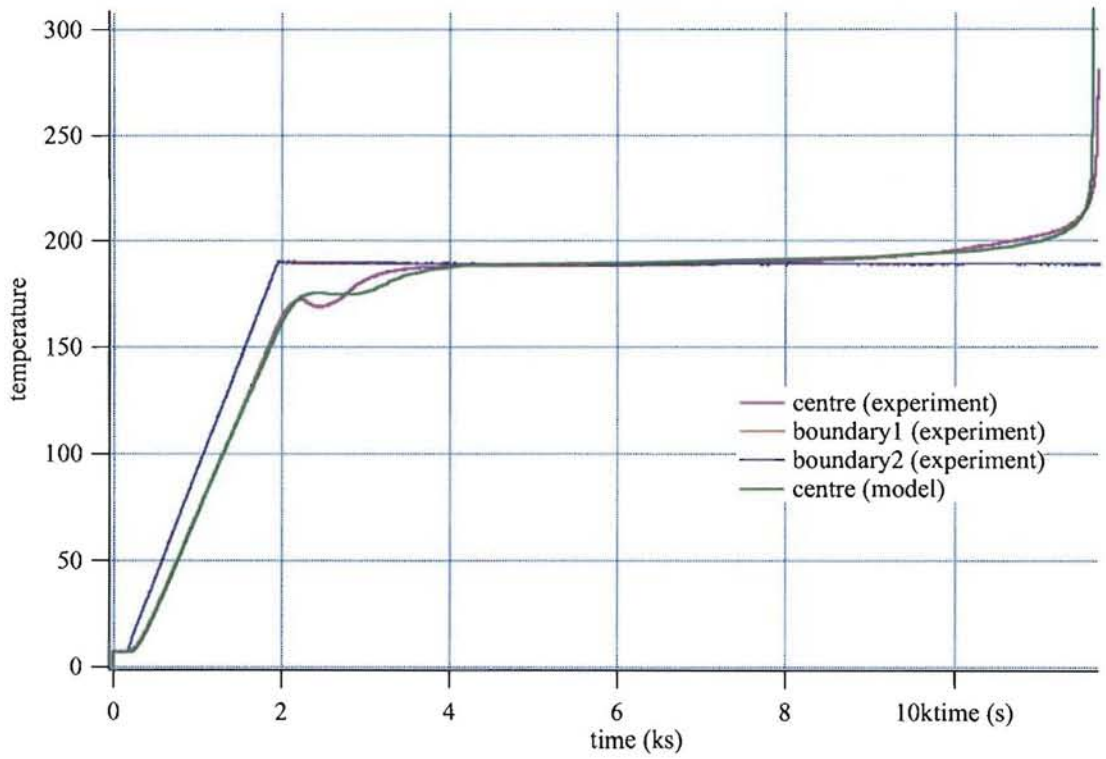
300
250
200
150
100
50
0
temperature
0
2
4
6
8
10ktime (s)
time (ks)
centre (experiment)
boundary1 (experiment)
boundary2 (experiment)
centre (model)

Figure 3

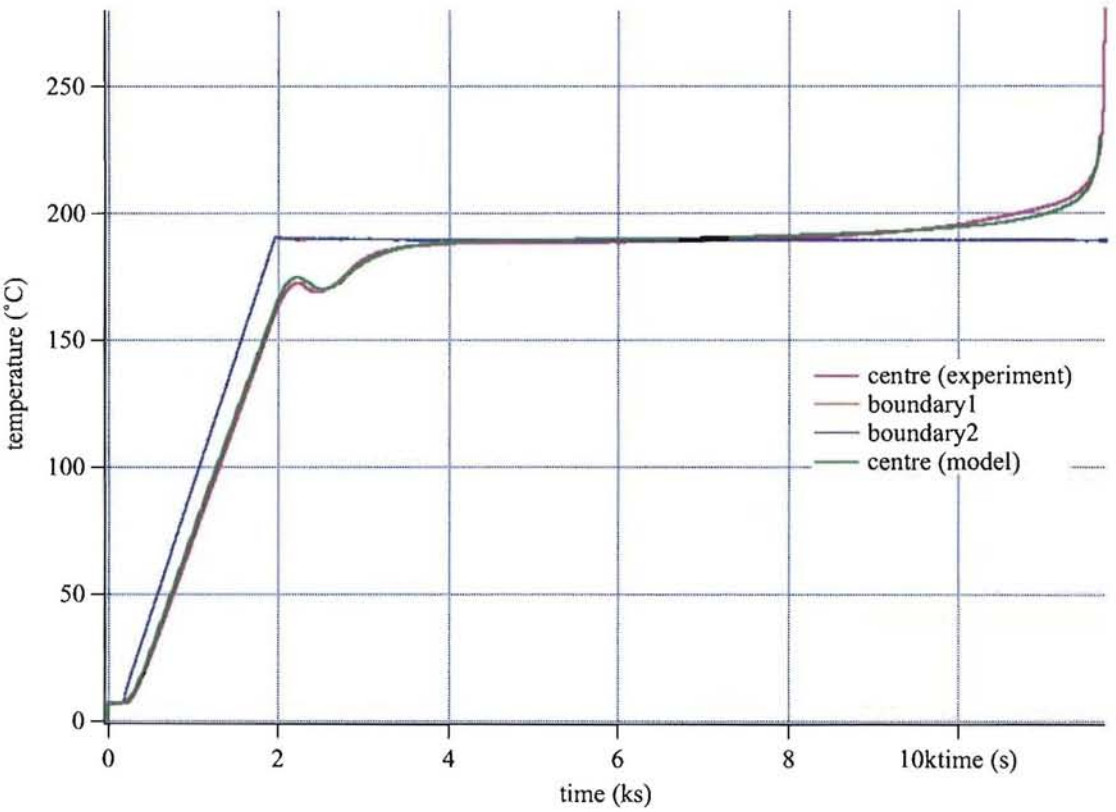
250
200
150
100
50
0
temperature (°C)
0
2
4
6
8
10ktime (s)
time (ks)
centre (experiment)
boundary1
boundary2
centre (model)

Figure 4

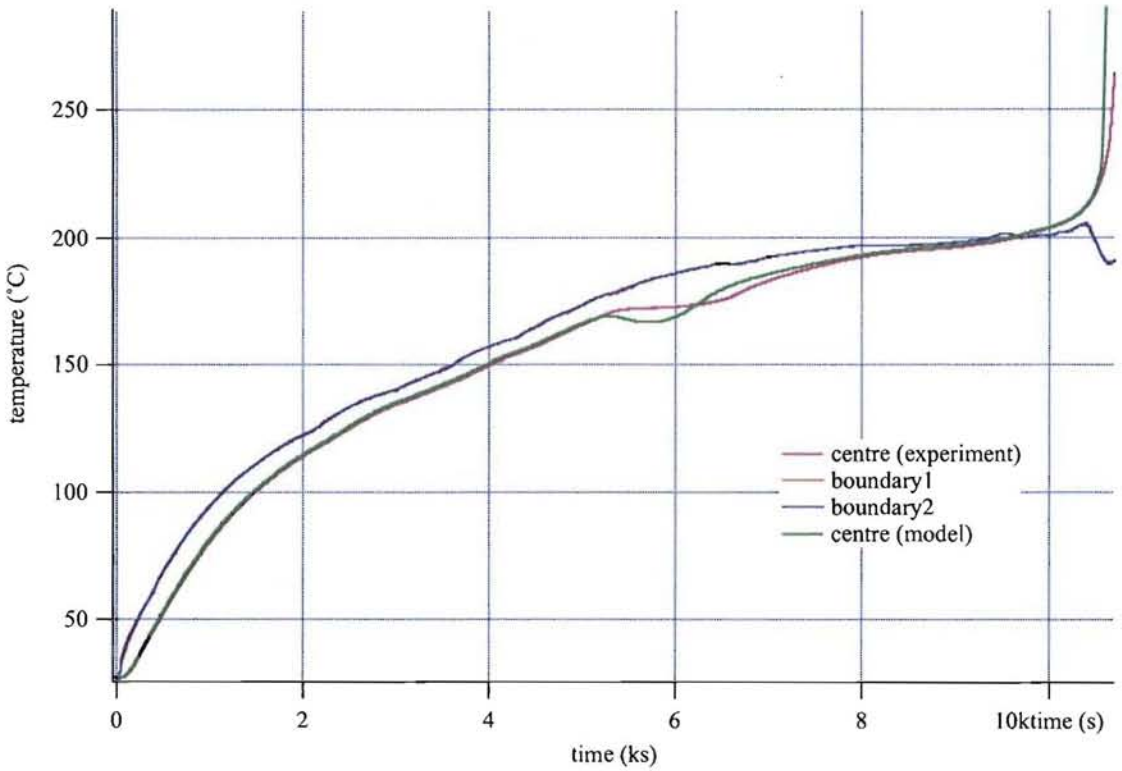
250
200
150
100
50
temperature (°C)
0
2
4
6
8
10ktime (s)
time (ks)
centre (experiment)
boundary1
boundary2
centre (model)

Figure 5. Schematic of the rail cart and anvil assembly.

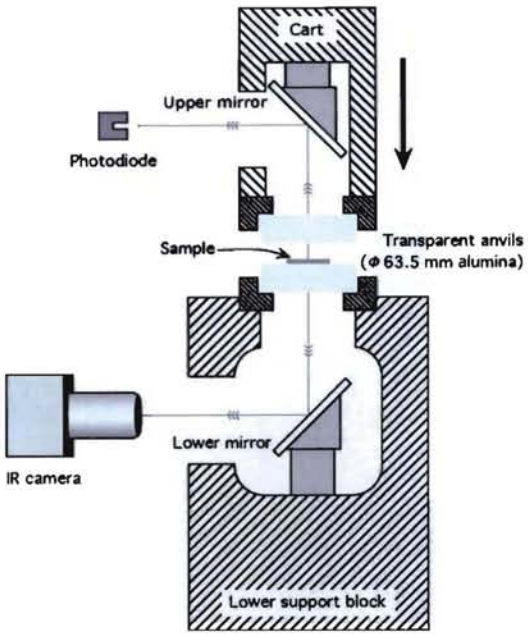

Figure 6. A typical load curve along with the photodiode signal. Note the change in slope of the load curve coincident with ignition.

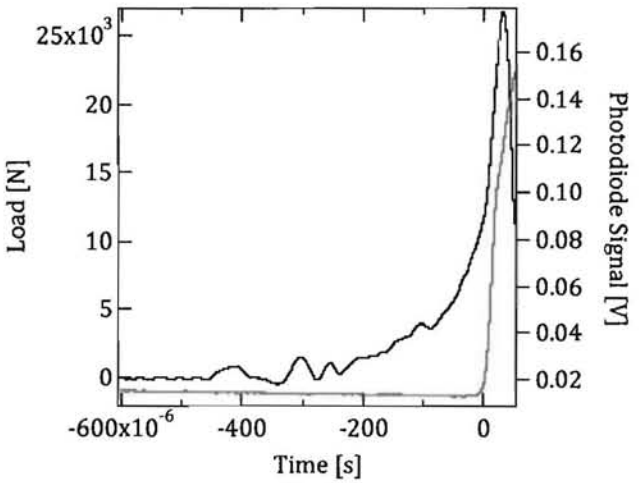

Figure 7.

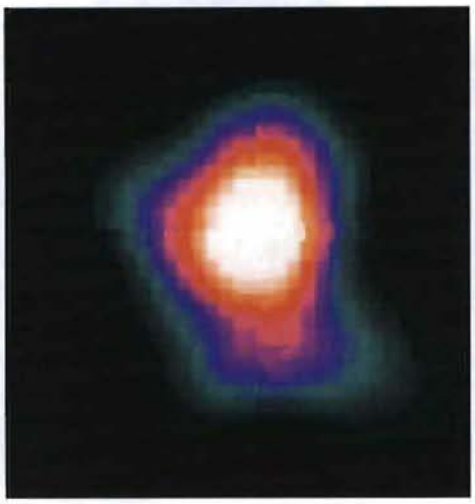

Figure 8: Meshed rendering of the system.

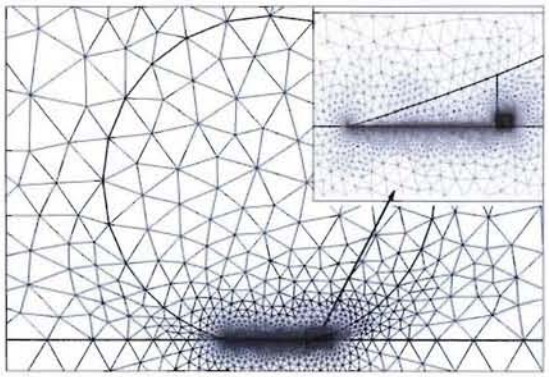

Figure 9. Radial grit velocity as a function of load.

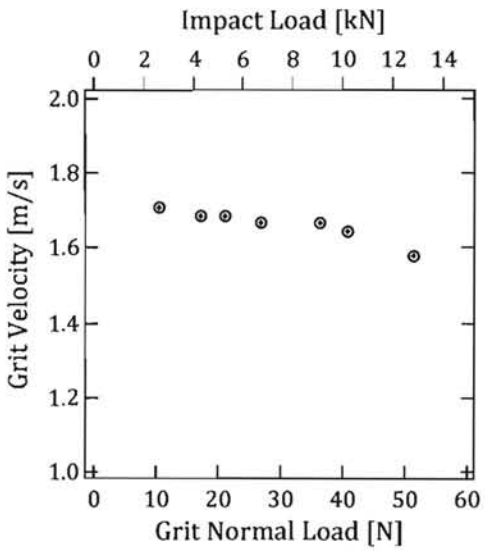

Figure 10. The average work rate versus time curve for all experiments.

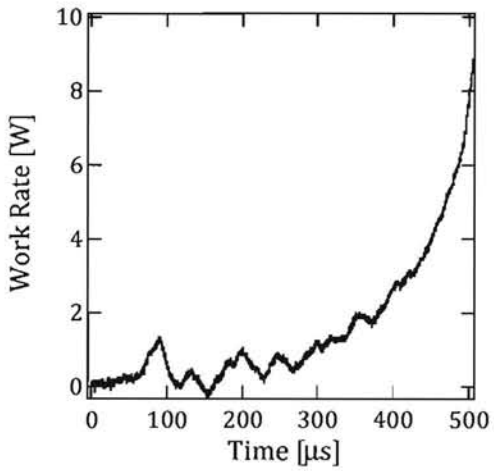

Figure 11: Temperature contour images at three zoom levels.

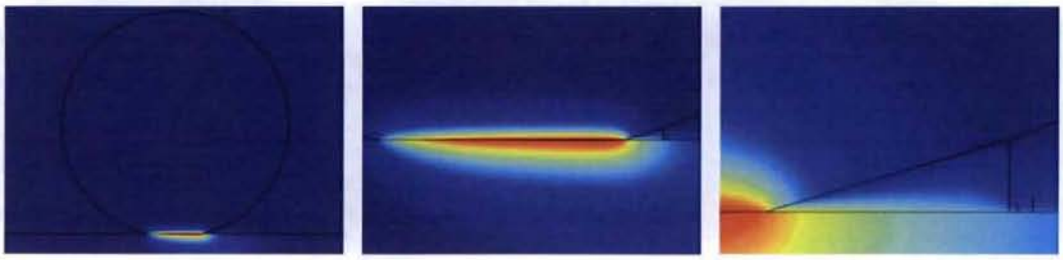

Figure 12: Time-temperature trajectory at the ignition location.

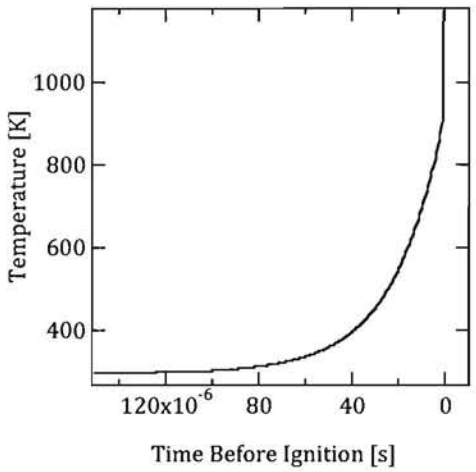

Figure 15: Behavior of the heat source term. Note the endothermic phase transition.